CONF-960815--3
SAND96-0725C

Thermal Response of Ceramic Components During Electron Beam Brazing*

T. E. Voth
S. E. Gianoulakis
J. A. Halbleib

Sandia National Laboratories
Albuquerque, NM

Submitted to:
Transport Phenomena During Processing of Polymeric and Ceramic Composites
1996 ASME National Heat Transfer Conference
Houston, Texas
August 3 - 5, 1996

* This work was supported by the United States Department of Energy under contract DE-AC04-94ALB5000.

Nomenclature

c	specific heat
H	height of alumina and braze part
i	beam current
k	thermal conductivity
n	surface normal
P	power
q''_f	furnace to assembly surface heat flux
Q_{dep}	energy deposition
r	radial coordinate
R	radius
t	time
t_{cool}	cooling time ($t_{final} - t_{off}$)
T	temperature
V	volume
z	axial coordinate

Greek Symbols

ΔT_{base}	temperature difference ($T_b - T_{base}$)
ε	emissivity
ρ	density

Subscripts

b	braze
base	base, located at $r = R_i$, $z/H = 1$
c	chuck
eb	electron beam

f	furnace
final	final
i	inner
m	melting
max	maximum
o	outer
off	beam off

Abstract

Ceramics are being used increasingly in applications where high temperatures are encountered such as automobile and gas turbine engines. However, the use of ceramics is limited by a lack of methods capable of producing strong, high temperature joints. This is because most ceramic-ceramic joining techniques, such as brazing, require that the entire assembly be exposed to high temperatures in order to assure that the braze material melts. Alternatively, localized heating using high energy electron beams may be used to selectively heat the braze material.

In this work, high energy electron beam brazing of a ceramic part is modeled numerically. The part considered consists of a ceramic cylinder and disk between which is sandwiched an annular washer of braze material. An electron beam impinges on the disk, melting the braze metal. The resulting coupled electron and thermal transport equations are solved using Monte Carlo and finite element techniques. Results indicate that increased electron beam current decreases time to melt as well as required cooling time. Vacuum furnace brazing was also simulated and predicted results indicate increased processing times relative to electron beam brazing

Introduction

Ceramics are being used increasingly in applications where high temperatures are encountered such as automobile and gas turbine engines (Frankhouser, 1987; ASM, 1991). However, the use of ceramics is limited by a lack of methods capable of producing strong, high temperature resistant ceramic-to-ceramic joints. This is, in part, because many ceramic-to-ceramic joining techniques, such as brazing, require that the entire assembly be exposed to temperatures greater than their expected service temperature during processing in order to ensure that the braze metal melts (Schwartz, 1987). One such brazing method involves heating the part in a vacuum furnace. In a number of applications, the ceramic assembly encloses temperature sensitive components (such as electronics). Additionally, the joined materials may be damaged by high furnace temperatures (Hammond, et al., 1988). Thus, for furnace processing, low melting temperature braze materials must be used.

Alternatively, localized heating using lasers or high energy electron beams (energies between 1 to 10 MeV) may be used to selectively heat the braze metal with neighboring components remaining relatively cool (Schwartz, 1987; Goodman et al., 1995; Turman et al., 1995). Electron beam processing has an advantage over laser processing because it can be "tuned" (by adjusting beam energy) to induce volumetric heating at locations within the part which cannot be reached by a laser beam (Goodman et al., 1995). Additionally, electron beam processing is expected to be ten to twenty times cheaper than laser processing (Turman, 1992).

A disadvantage of using localized heating relative to furnace processing is that large temperature gradients produced in the part may crack the ceramic. Lower heating rates may be used to reduce gradients and minimize cracking at the expense of increased production time. Additionally, since the braze must still reach melting temperature, lower heating rates result in increased volume-averaged part temperature, and thus reducing the advantages of this method relative to furnace brazing.

In this work, high energy electron beam brazing of a ceramic part is modeled numerically. Parametric simulations are performed to investigate the effect of electron beam current (and hence power) on part thermal response. To assess the advantages of electron beam brazing, the predicted thermal response of the brazed ceramic part is compared to the response for vacuum furnace processing.

Numerical Model

The assembly geometry considered here is illustrated in Figure 1 and is designed to simulate a production facility under development at Sandia Laboratories. The assembly consists of the ceramic part mounted on a 7 mm thick disk of zirconium dioxide and a 6.4 mm thick aluminum chuck both of radius $R_c = 50.8$ mm. The zirconium dioxide serves as thermal insulation and as an absorber for stray electrons while the aluminum disk provides mechanical rigidity for the assembly. The part consists of an alumina tube ($R_i = 7.62$ mm, $R_o = 12.7$ mm) and a disk 5.08 mm thick between which is a braze washer 0.08 mm thick. The part height, H, is 30.7 mm. For the analysis, the assembly and boundary conditions are assumed to be axisymmetric. Properties of the assembly materials may be found in Table 1.

The thermal response of the assembly was predicted using a one-way coupled electron transport-thermal analysis. This was accomplished by first predicting the temperature independent electron transport within the assembly using a Monte Carlo code. The resulting energy deposition rates were then mapped onto the finite element nodes for the thermal analysis as energy generation terms. The electron-transport equations were solved using the Integrated Tiger Series (ITS) code. ITS is a time-independent coupled electron-photon Monte Carlo code that simulates the production and transport of the electron-photon cascade. Details concerning ITS are available elsewhere (Halbleib, 1988; Halbleib et al, 1992). The thermal analysis was performed using COYOTE II (Gartling and Hogan, 1994). COYOTE II is a finite element code for

solving the non-linear, heat diffusion equation. Phase change of the braze material was not simulated.

Thermal boundary conditions were modeled as gray body radiation from the part to the surroundings which were assumed to be maintained at 300 K. The part was assumed to be initially at 300 K with the electron beam off. At t = 0 the beam was turned on. The beam was simulated as an annular source of uniform 10 MeV electron kinetic energy centered at $r = (R_i+R_o)/2$ with a width of 5.08 mm, impinging on the part at z/H = 0 as shown in Figure 1. The beam was on until the braze temperature, T_b, at a location in the center of the braze washer (braze temperature varies spatially by less that 1 K due to its relatively high thermal conductivity, see Table 1) reaches $T_{off} = T_m + 10$ K (to ensure melting). The beam was then turned off and the assembly was allowed to cool radiatively.

Numerical experiments were performed to determine sensitivity of the results to mesh size. The number of elements, for the electron transport and thermal analysis, were doubled simultaneously until $T_{b,max}$ changed by less than 1 percent between subsequent mesh refinements. A total of 440 Monte Carlo elements and 2200 quad elements where found to satisfy these requirements and were used for the following analysis. Finally, the Monte Carlo simulations presented here incorporated 400,000 electron histories resulting in an estimated 1-σ statistical uncertainty of approximately 1% over most of the geometry.

Results and Discussion

Parametric simulations for a range of beam currents, i, have been performed. Beam currents of 20, 60, and 100 μA were investigated as they are typical of the range of commercial beams available (Turman et al., 1995). Electron transport predicted energy generation results are discussed first. Base-case thermal analysis results are then presented, followed by a comparative study of the effects of varying beam current on the

thermal response of the part relative to the base case. Finally, a comparison of part thermal response for both electron beam and furnace processing is made.

Electron beam energy deposition

Figure 2 shows the energy deposition distribution in the alumina and braze at r = 10.2 mm (halfway between R_i and R_o). Energy absorbed scales linearly with beam current (as well as atomic number) and thus is normalized with i. Maximum energy deposition occurs in the braze material due to its higher atomic number relative to the alumina resulting in more rapid heating of the braze. Energy deposition decreases with increased z/H for $z/H > 0.17$ as the electron beam energy is attenuated. Figure 3 shows the energy deposition contours in the alumina part. Interestingly, the deposition contours are quite asymmetric about $r = (R_i + R_o)/2$, particularly for $z/H > 0.25$. This is due, in part, to portions of the beam which scatter out, and are reflected back into the part from the axis of symmetry.

Base case thermal response

The 100 μA case was arbitrarily chosen for the base case. Figure 4 shows the base case T_b history. During the heating phase, T_b increases rapidly, with $\partial T_b/\partial t$ decreasing with increasing T_b due to conductive losses to the cooler portions of the assembly and radiative losses to the surroundings. Once T_b reaches T_{off}, the electron beam is turned off and the part cools.

The temperature difference, ΔT_{base}, between T_b and a point at $r = R_i$, $z/H = 1$ is also shown in Figure 4 and illustrates the localized nature of electron beam heating. Initially, the assembly is at room temperature and ΔT_{base} is zero. After the electron beam is turned on ($t > 0$) ΔT_{base} begins to increase and reaches a maximum of approximately 480 K at t = 16 s. After the beam is turned off ($t > 16$ s) part temperatures equilibrate and ΔT_{base} approaches zero.

Figure 5 (a) displays the temperature contours in the part when $T_b = T_m$ (t = 15 s). Minimum and maximum contours are indicated, and each intermediate contour represents a 50 K increment. The figure again illustrates the large temperature gradients in the part, with a temperature difference of approximately 500 K from z/H = 0 to 1.

Thermal response for all cases

The brazing process can be divided into heating and cooling stages. The effects of beam current, i, on the thermal response of the part during these stages is presented in Figure 6. Figure 6 (a) shows the braze temperature thermal history for several different i, and several trends are evident. During the heating stage, $\partial T_b/\partial t$ is a function of i. This is because beam volumetric energy deposition (and hence Q_{dep}) scales linearly with beam current (see Figs. 2 and 3). In addition to increasing the heating rate, increased beam current also slightly decreases cooling times, t_{cool} ($t_{cool} = t_{final} - t_{off}$). This is due, in part, to decreased energy deposition in the part as a result of reduced heating time.

Figure 6 (b) illustrates the effect of increased i on temperature gradients in the part. As i decreases from 100 to 20 μA, $\Delta T_{base,max}$ is reduced to approximately half. This reduction in $\Delta T_{base,max}$ is due to increased thermal diffusion (due to increased heating times), resulting in more uniform part temperatures relative to the base case. Figure 5 (b) displays temperature contours in the part when $T_b = T_m$ (t = 193 s) and illustrates this reduction in part temperature gradients for the 20 μA case. Minimum and maximum contours are indicated, and each intermediate contour represents a 20 K increment.

Comparison to vacuum furnace processing

In the previous discussion, it has been shown that electron beam processing is capable of producing very localized heating. To emphasize the advantages of electron beam processing relative to standard ceramic-to-ceramic brazing techniques a comparison is made to vacuum furnace brazing.

Vacuum furnace brazing is modeled by assuming that the entire assembly is subjected to a uniform heat flux (the heat transfer mode is not specified). Thus the thermal boundary condition due to furnace heating is

$$k\frac{\partial T}{\partial n} = q''_f \bullet n \qquad (1)$$

where q''_f is the furnace supplied surface heat flux which is evaluated as follows.

In order to make a comparison between electron beam and furnace heating, the electron beam power absorbed by the part, P_{eb}, is set equal to the power supplied by the furnace, P_f. The electron beam power absorbed may be found by integrating Q_{dep} over the assembly volume. Thus, P_{eb} = 166, 497 and 829 W for the 20, 60 and 100 μA cases respectively. The comparable furnace heat flux is calculated as $q''_f = P_{eb}/A$ where A is the assembly's exposed surface area (= 1.123×10^4 mm^2). The resulting values for q''_f are then 0.01476, 0.04427 and 0.07379 W/mm^2 for the 20, 60 and 100 μA cases respectively. Note that q''_f = 0.07 W/mm^2 for actual vacuum furnace processing. An additional case of i = 35 μA (P_{eb} = 290 W, q''_f = 0.02583 W/mm^2) is introduced for completion.

The thermal responses for the electron beam and vacuum furnace base cases (P_{eb} = 829 W) are shown in Figure 7. Figure 7 (a) compares furnace and electron beam T_b histories and shows that during the heating phase electron beam processing induces significantly greater $\partial T_b/\partial t$. This is because electron beam heating increases the temperature of less assembly mass relative to the furnace case. Figure 7 (b) shows ΔT_{base}, further demonstrating the localized heating produced by electron beam processing relative to furnace brazing. The electron beam $\Delta T_{base,\,max}$ is 3.7 times that of the furnace case. The remaining furnace and electron beam case $\Delta T_{base,\,max}$ values are shown in Figure 8. It is evident from the figure that increasing P results in an increase in the difference between the furnace and electron beam $\Delta T_{base,\,max}$ values.

Because processing time can affect final part cost, significant effort has been devoted to reducing vacuum furnace processing time (Schwartz, 1987). It is therefore of interest to compare electron beam and furnace processing times. Figure 9 (a) shows the time required to reach T_m , t_m, for both electron beam and furnace processing. As P decreases, both electron beam time-to-melt, $t_{m,eb}$ and furnace time-to-melt $t_{m,f}$ increase as expected. Interestingly, $t_{m,eb}$ and $t_{m,f}$ diverge as P decreases, with furnace heating requiring approximately 10 times longer to reach T_m at P = 290 W. Note that a P = 166 W case is not shown for furnace processing in Figures 8 and 9. This is because this power level was not high enough to overcome radiative losses, resulting in a steady state $T_b < T_m$.

Time-to-cool, t_{cool}, defined as $t_{cool} = (t(T_{cool}) - t_m)$ is shown in Figure 9 (b) (T_{cool} is arbitrarily taken to be 600 K). Similar trends as in Fig. 9 (a) are noted with decreased P increasing $t_{m,f}$ and $t_{m,eb}$ while also increasing their separation. Furnace heating requires approximately 8 times longer to reach T_{cool} at P = 290 W. This increased cooling time results as more energy is deposited in the assembly during furnace heating.

Conclusions

A numerical model has been used to investigate the effects of beam current on the thermal response of a part during high energy electron beam brazing. Beam current was varied for given part dimensions and thermal boundary conditions. For the part considered, the results showed that increasing beam current increased heating rate and decreased time to melt as well as decreased cooling time. Vacuum furnace brazing was also simulated and results show that this popular brazing method required longer melting and cooling times than electron beam brazing. The results suggest that processing times can be reduced with electron beam brazing.

References

ASM, 1991, *Engineering Materials Handbook, Ceramics and Glasses*, ASM International, Metals Park, Ohio.

Frankhouser, W. L., 1987, *Advanced Processing of Ceramic Compounds*, NDC, New Jersey.

Gartling, D. and Hogan, R., 1994, *Coyote II - A Finite Element Computer Program for Nonlinear Heat Conduction Problems,* Sandia Report Number SAND94-1179, Sandia National Laboratories, Albuquerque.

Goodman, D. L., Birx, D. L. and Dave, V. R., 1995, "High Energy Electron Beam Processing Experiments with Induction Accelerators," *Nuclear Instruments and Methods in Physics Research B*, Vol. 99, pp. 775-779.

Glass, S. J., 1995, private communication, Sandia National Laboratories, Albuquerque.

Halbleib, J. A., 1988, "Applications of the ITS Codes," in *Monte Carlo Transport of Electrons and Photons*, Jenkins, T. M., Nelson, W. R. and Rindi, A., Plenum Press, New York.

Halbleib, J. A., Kensek, R. P., Valdez, G. D., Seltzer, S. M. and Berger, M. J., 1992, "ITS: The Integrated TIGER Series of Electron/Photon Transport Codes - Version 3.0," *IEEE Transactions of Nuclear Science*, Vol. 39, pp. 1025 - 1030.

Hammond, J. P., David, S. A. and Santella, M. L., 1988, "Brazing Ceramic Oxides to Metals at Low Temperatures," *Welding Journal*, Vol. 67, pp. 227s-232s.

Incropera, F. P. and DeWitt, D. P., 1985, *Fundamentals of Heat and Mass Transfer*, 2nd ed., John Wiley & Sons, New York.

Lamarsh, J. R., 1983, *Introduction to Nuclear Engineering*, 2nd ed., Addison-Wesley, Reading.

Schwartz, M. M., 1987, *Brazing*, ASM International, Metals Park, Ohio.

Touloukian, Y. S., 1967, *Thermophysical Properties of High Temperature Solid Materials*, Vol. 4, The Macmillan Co., New York.

Turman, B. N., 1992, "Fundamentals of High Energy Electron Beam Generation," in *Proceedings, High-Energy Electron-Beam Welding and Materials Processing Conference*, ASM, Metals Park, Ohio.

Turman, B. N., Glass, S. J., Halbleib, J. A., Helmich, D. R. and Loehman, R. E., 1995, *Electron Beam Joining of Structural Ceramics*, Sandia Report Number SAND95-0595.

Wesgo, 1993, *Technical Ceramics and Brazing Alloys Data Sheets*, Wesgo Inc., Belmont, CA.

Figure Captions

Figure 1 - Schematic of the geometry.

Figure 2 - Part energy generation per unit beam current distribution at r = 10.2 mm, $0 \leq Z/H \leq 1$. Units are in $W/mm^3 \bullet \mu A$

Figure 3 - Energy generation per unit beam current contours within the cylindrical section and cap. Contours are in 0.25×10^{-3} $W/mm^3 \bullet \mu A$ increments.

Figure 4 - Base case (i = 100 μA) thermal response showing (a) braze temperature and (b) braze to base (base location is $r = R_i$, $z/H = 1$) temperature difference histories.

Figure 5 - Part temperature contours (in Kelvins) at $t = t_m$ for (a) the base case (i = 100 μA) and (b) the i = 20 μA case. Minimum and maximum contours are shown and temperature increments are 5 K and 50 K for (a) and (b) respectively.

Figure 6 - Transient thermal response histories for (a) braze temperature and (b) braze to base temperature difference for 20, 60, and 100 μA cases.

Figure 7 - Comparison of electron beam and vacuum furnace base case transient thermal response histories for (a) braze temperature and (b) braze to base temperature difference.

Figure 8 - Comparison of electron beam and vacuum furnace maximum braze to base temperature difference for a range of power input.

Figure 9 - Comparison of electron beam and vacuum furnace (a) time to melt and (b) cooling time for a range of power input.

Table 1 - Properties used for the predictions.

material	k (W/m•K)	c (J/kg•K)	ρ (kg/m^3)	T_m (K)	ε
alumina	25.6 [a]	795 [a]	3720 [a]	---	0.6 [a]
aluminum	237 [b]	903 [b]	2702 [b]	---	0.03 [b]
braze	280 [c]	280 [c]	9120 [c]	880 [c]	0.3
zirconium dioxide	2.1 [d]	628 [d]	5700 [d]	---	0.6 [d]

a Wesgo, 1993

b Incropera and DeWitt, 1985

c Glass, 1995

d Touloukian, 1967

e Lamarsh, 1983

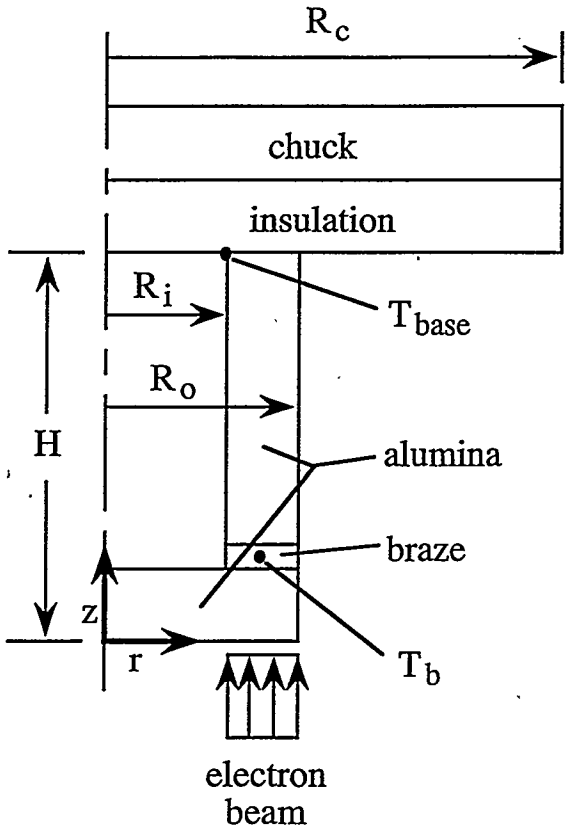

Figure 1 - Voth et al.

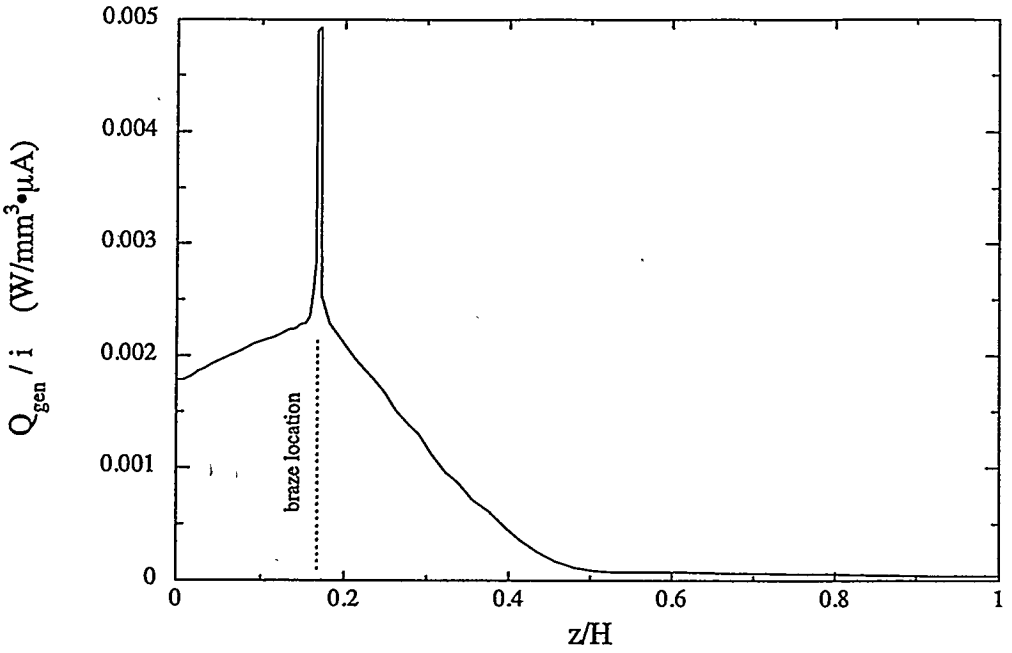

Figure 2 - Voth et al.

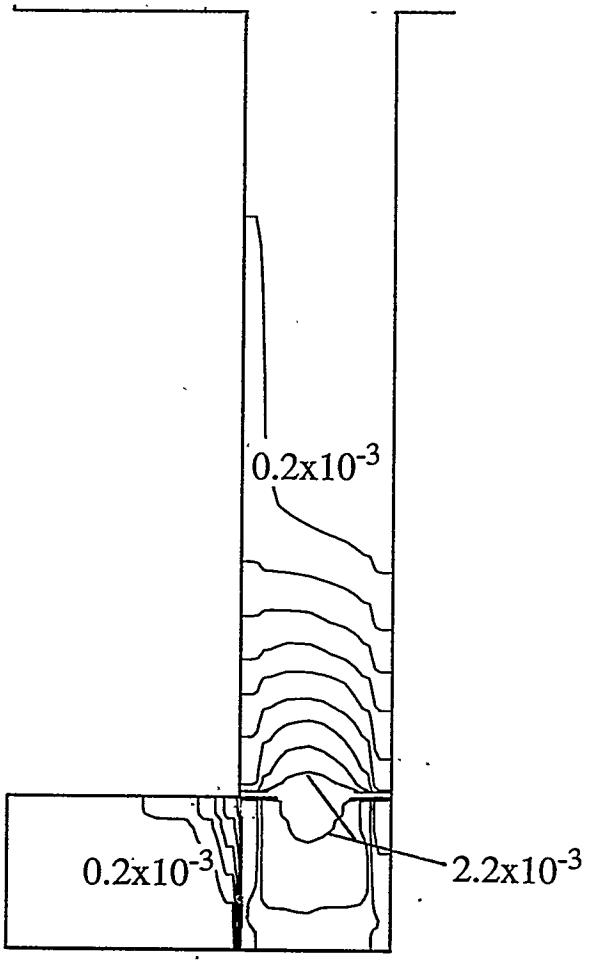

Figure 3 - Voth et al.

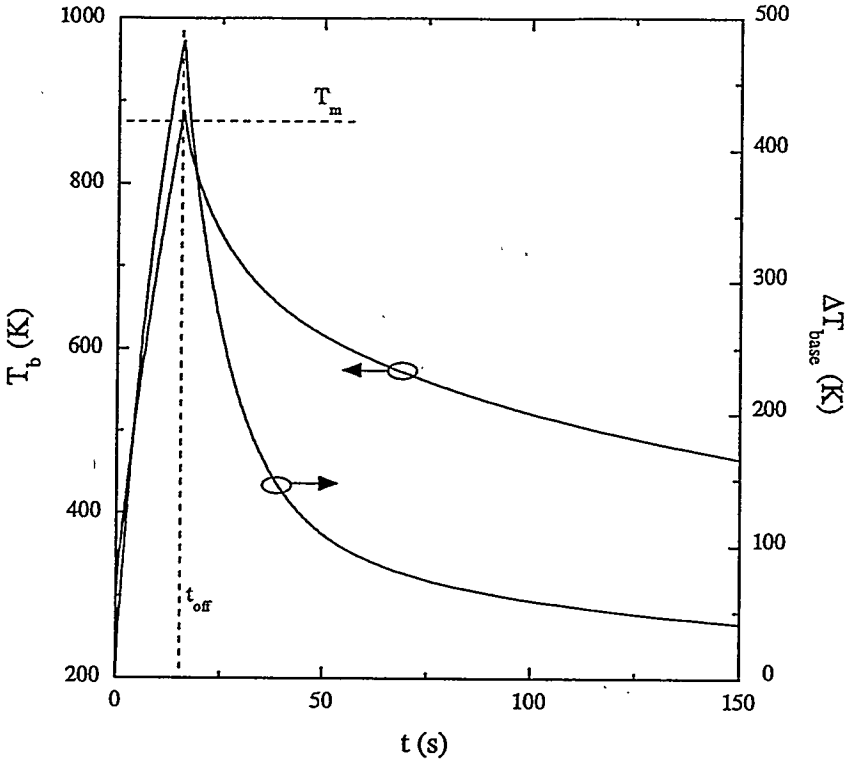

Figure 4- Voth et al.

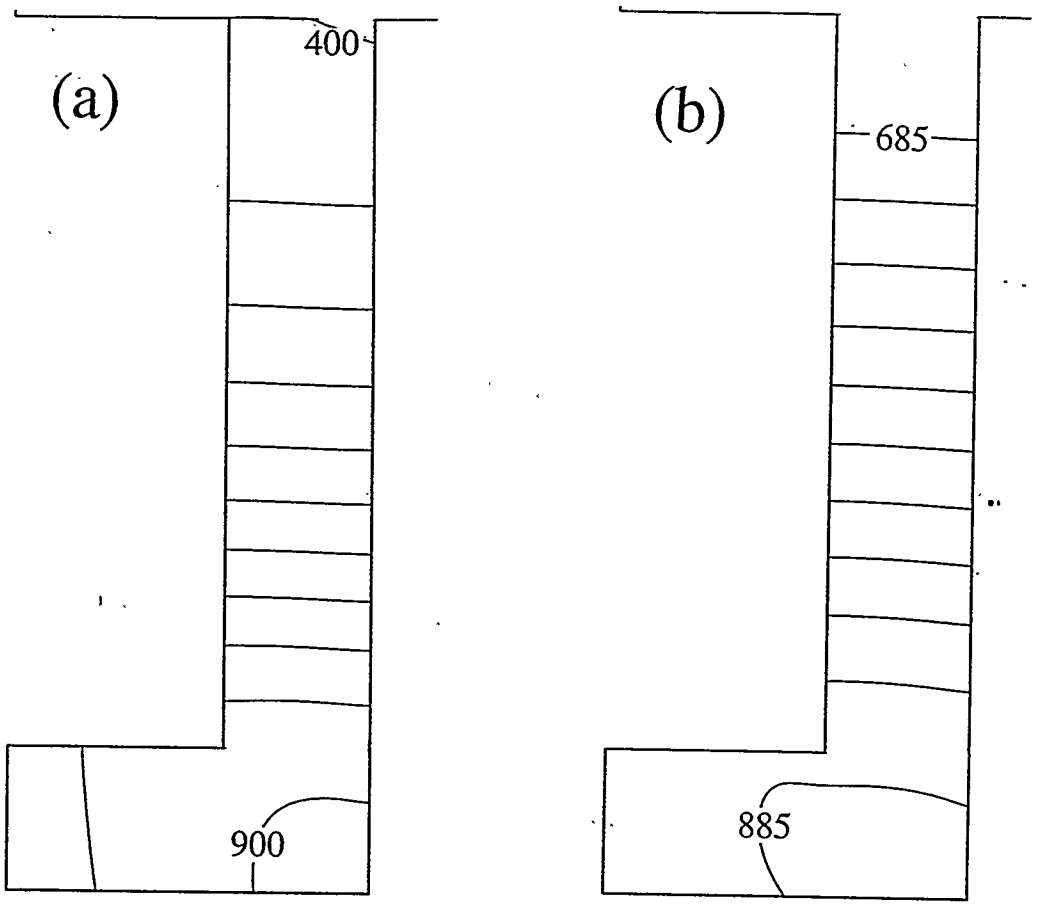

figure 5 - Voth et al.

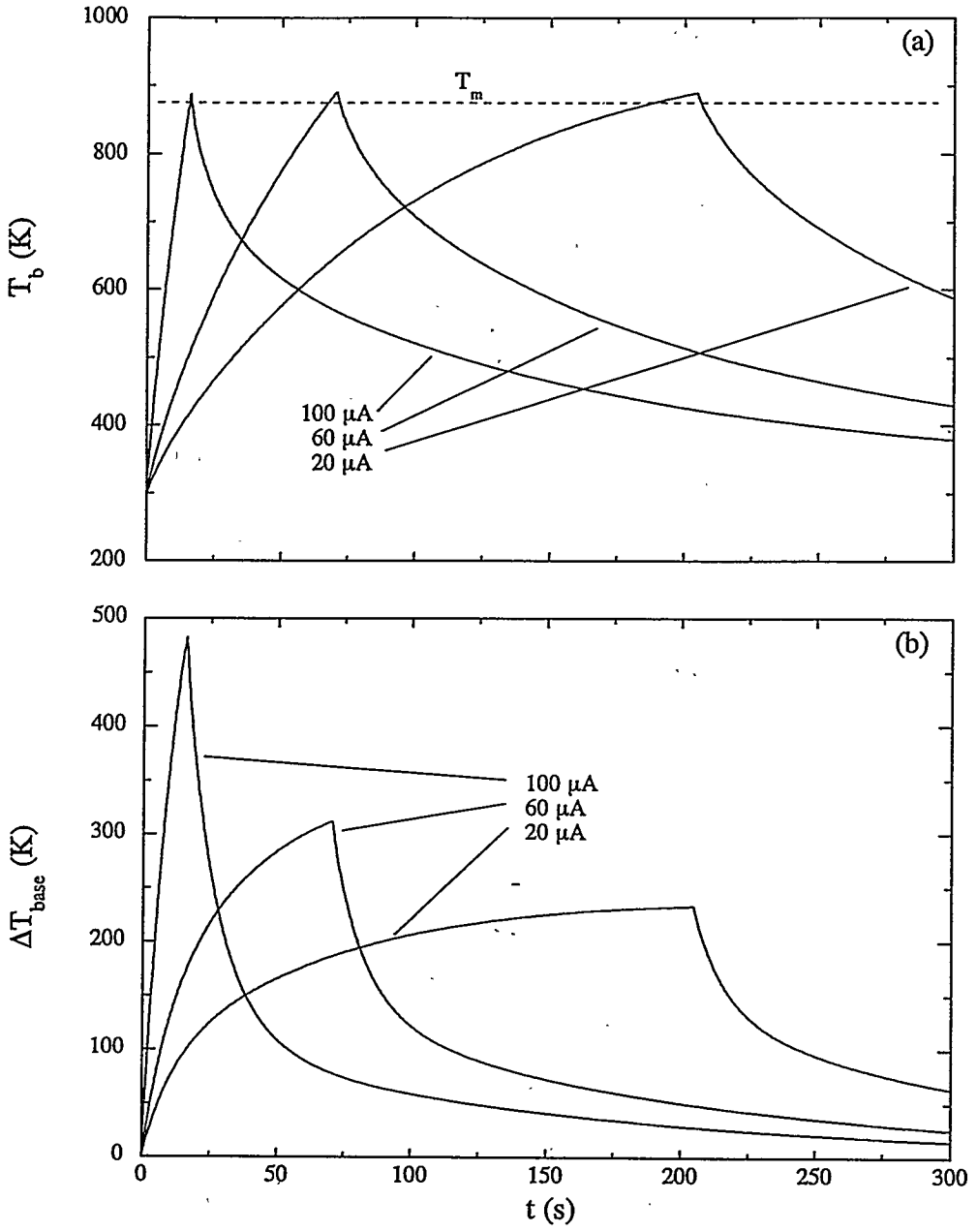

Figure 6 - Voth et al.

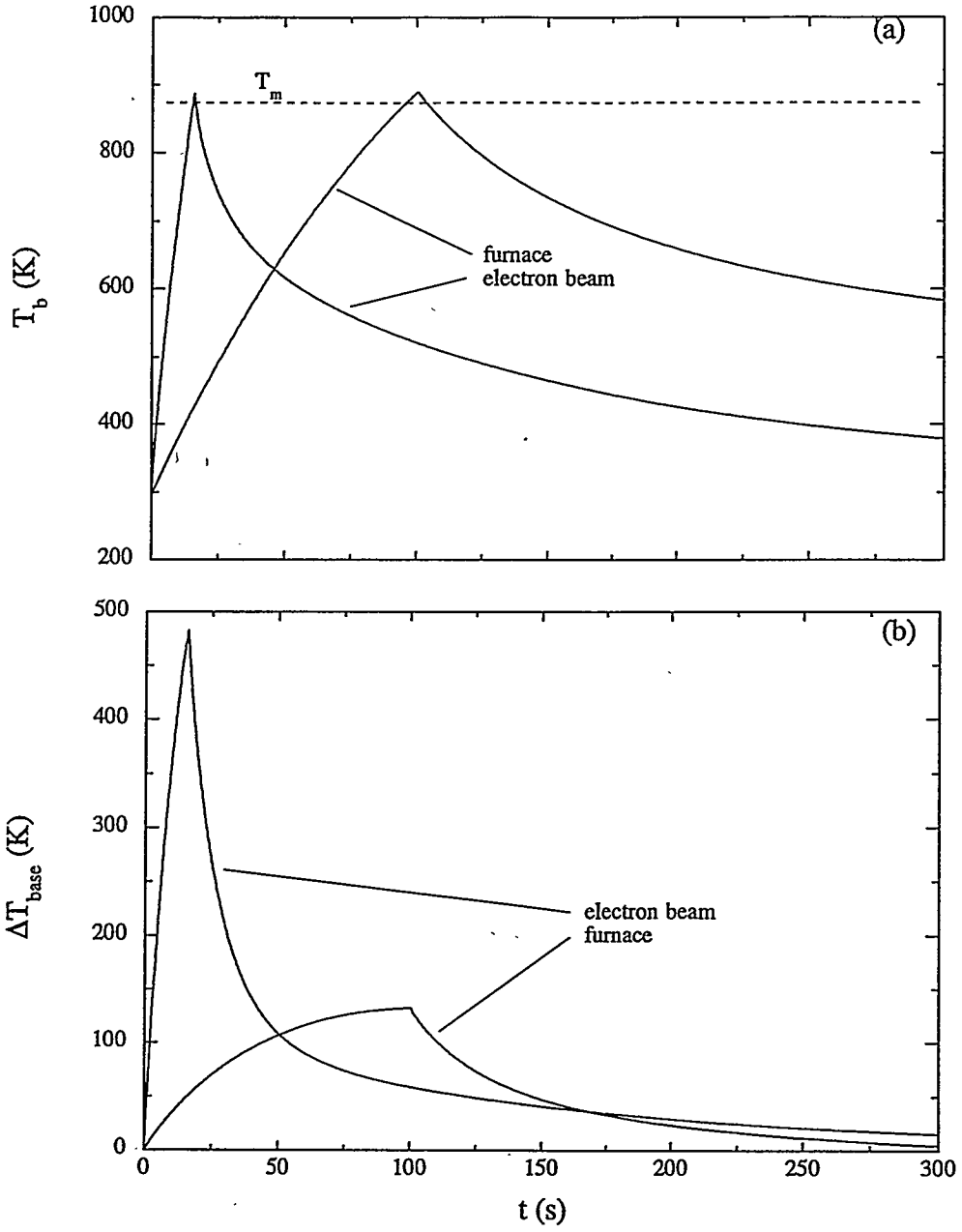

Figure 7- Voth et al.

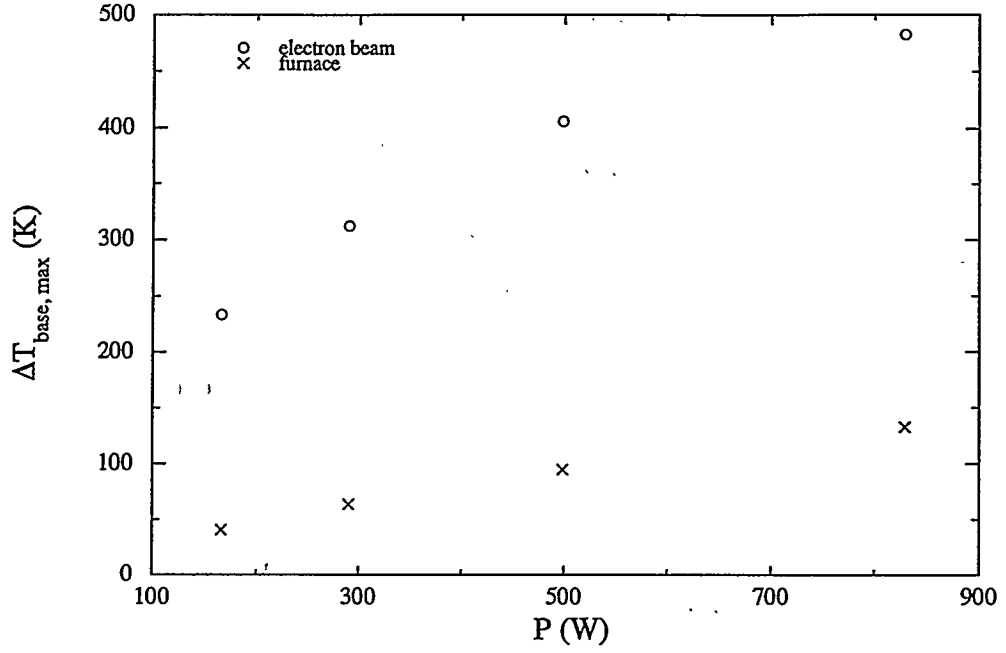

Figure 8 - Voth et al.

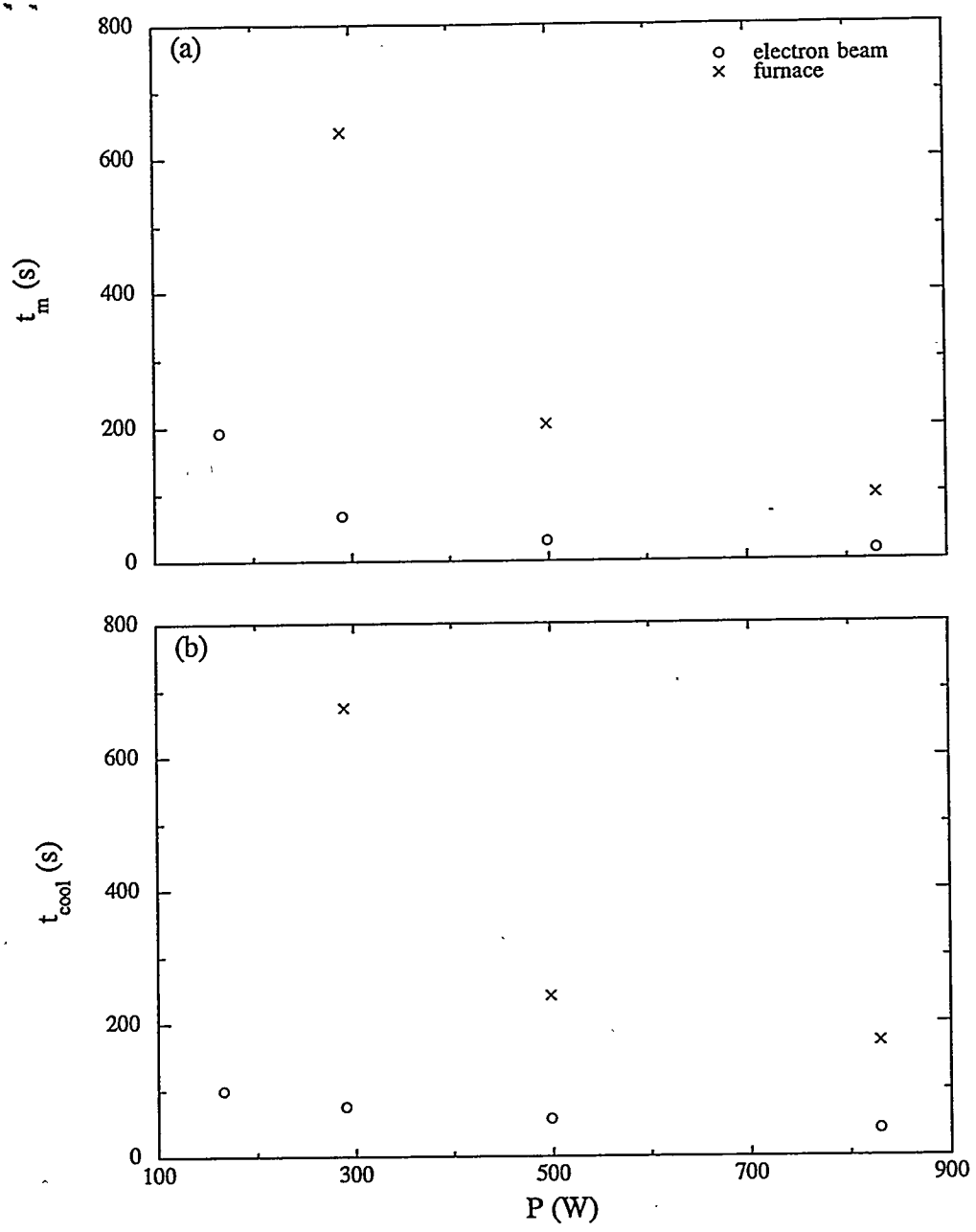

Figure 9 - Voth et al.